Effect of inflow density on ion diffusion region of magnetic reconnection: Particle-in-cell simulations

P. Wu,[1,a)] M. A. Shay,[1,b)] T. D. Phan,[2,c)] M. Oieroset,[2] and M. Oka[2]
[1]*Department of Physics and Astronomy, Bartol Research Institute, University of Delaware, 217 Sharp lab, Newark, Delaware 19716, USA*
[2]*Space Science Laboratory, University of California, Berkeley, California 94720, USA*

(Received 12 June 2011; accepted 22 August 2011; published online 29 September 2011)

We perform a systematic study of the effect of inflow density on reconnection diffusion regions using a 2.5-D particle-in-cell code. The diffusion region structures are analyzed at times when all simulations have reconnected the same amount of magnetic flux. We find that reducing the inflow density from 1 to 1/100th of the current sheet density dramatically increases the diffusion region physical size and the reconnection rate. The width of the diffusion region scales with the upstream ion inertial length systematically. Consistent with the presence of counter-streaming inflowing ion beams near the x-line, the ion meandering width in the diffusion region also scales with the ion inertial length. The aspect ratio of the ion diffusion region remains a constant, independent of the inflow density. The quadrupole Hall magnetic field is reduced. The upstream magnetic field deviates from its asymptotic value by ~50% at the lowest simulated inflow density. The downstream ion outflow velocity scales linearly with the upstream Alfvén speed with a multiplication factor $\sim 0.4 < 1$. When applied to magnetic reconnection in the Earth's magnetotail, this factor of 0.4 is a possible explanation as to why bulk flow velocities in the magnetotail are typically on the order of 500 km/s, while the Alfvén speeds of inflowing plasmas can exceed 2000 km/s. © *2011 American Institute of Physics*. [doi:10.1063/1.3641964]

I. INTRODUCTION

Magnetic reconnection drives explosive events in the magnetosphere[1] and on the solar surface.[2] It also disrupts fusion experiments in the laboratory.[3] The breaking of magnetic topology during reconnection is achieved inside the diffusion region, where plasmas de-couple from the magnetic field lines and the field lines re-organize themselves. Because the diffusion region contains the essential physical processes that lead to the breaking of the field lines, understanding the basic physics of the diffusion region is important for understanding magnetic reconnection in general. As such, the reconnection diffusion region has been the focus of intense numerical study. Many computational studies of undriven reconnection have found that the diffusion region aspect ratio is independent of system size and the effective mechanism that breaks the frozen-in condition (e.g., Refs. 4 and 5). However, the cause of this independence of the reconnection has been a matter of controversy (e.g., Refs. 6–8). Other studies, typically driven, have seen a system size dependence on the reconnection rate (e.g., Refs. 9–12). In this paper, we focus on undriven magnetic reconnection.

In the undriven regime, despite the diffusion region properties for electron-ion plasmas have been the subject of much scrutiny, a systematic understanding of the inflow density effect on the diffusion region is lacking. In the large majority of previous reconnection simulation studies using Harris type equilibrium current sheets (e.g., the GEM challenge study[5]), the density in the inflow region was relatively large, being only about a factor of six times smaller than the density in the equilibrium current sheet. In many physical plasmas, however, such as those found in the Earth's magnetotail, the density outside of the equilibrium current sheet can be extremely low, with inflow density a factor of 100 lower than the equilibrium current sheet density.[13] Will such low inflow density cause a fundamental change in reconnection? Such low densities typically require the use of kinetic particle-in-cell (PIC) simulations, which are computationally more expensive than fluid simulations.

Previously, reconnection with zero inflow density was simulated in one of the GEM-challenge studies.[14] The reconnection rate was greatly accelerated, with a rate of $E_R \sim 2B_\infty v_{A0}/c$, where E_R is the out of the plane reconnection electric field, B_∞ is an asymptotic magnetic field in the simulation, v_{A0} is the Alfvén speed calculated from the asymptotic magnetic field and the maximum current sheet density n_0, and c is the speed of light. Another study simulated an inflowing density 100 times smaller than the current sheet density, finding impulsive magnetic reconnection associated with a broadening of the diffusion region.[15] Comparing electron-proton like (mass ratio 25) plasmas with electron-positron plasmas (pair plasmas), the reconnection electric field was found to be balanced by non-gyrotropic electron pressure for the electron-ion case and electron inertial for pair plasmas.[15]

A Sweet-Parker type analysis of the diffusion region yields the following reconnection outflow and reconnection rate:[16,17]

[a)]Electronic mail: penny@udel.edu.
[b)]Electronic mail: shay@udel.edu.
[c)]Electronic mail: phan@ssl.berkeley.edu.

$$v_{io} = v_{A,up}, \tag{1}$$

$$E_R \sim \frac{\delta}{L} B_{up} \frac{v_{A,up}}{c}, \tag{2}$$

where v_{io} is the ion outflow speed, $v_{A,up}$ is the Alfvén speed determined from conditions just upstream of the diffusion region, δ and L are the width and length of the diffusion region, and B_{up} is the magnetic field just upstream of the diffusion region. Thus, a substantial reduction in the inflow density is expected to increase $v_{A,up}$, significantly increasing the reconnection rate. However, there are important unanswered questions. (1) For extremely low inflow densities, the low density outflow must somehow push the very high density equilibrium current sheet downstream. Although this may only be a transient effect, there is the possibility of back pressure and/or instability which could feed back and modify the diffusion region. (2) Will the aspect ratio δ/L change as the density is varied? Perhaps the back pressure from the equilibrium current sheet could change this? Examining the effect of varying inflow density on the ion diffusion region is the focus of this manuscript.

In the previous simulation for the pair plasma case,[15] the effect of inflow density variation was also examined. At inflow density 100 times smaller than the current sheet density, the authors find faster reconnection and broader diffusion region that suppresses secondary islands. The authors also show that the outflow speed is reduced to 0.2–0.3 of the upstream Alfvén speed. They interpret the results as the breakdown of Eq. (1) at small densities. Furthermore, they find that the aspect ratio of the diffusion region δ/L becomes much larger as the inflow density is decreased.

In the paper, we examine the effect of varying inflow density for electron-proton like plasmas with a mass ratio $m_i/m_e = 25$. Fully electromagnetic kinetic-PIC simulations are performed with relativistic effects included. The reconnections simulated are all anti-parallel. As the inflow density is lowered, the onset of magnetic reconnection occurs earlier and the reconnection rate is enhanced, as is expected. The width of the ion diffusion region is determined using the out of plane ion flow and is found to systematically scale with the upstream ion inertial length. The ion meandering length is also analyzed and found to systematically scale with the upstream ion inertial length, although being about a factor of two smaller. It is also seen systematically that the ion meandering Larmor radius equals ion meandering width. The ion scale diffusion region structure, i.e., the aspect ratio and the ion outflow velocity, is compared with the predictions of a Sweet-Parker-like scaling analysis of the diffusion region. We find that the outflow velocity scales with the Alfvén speed just upstream of the diffusion region, although reduced by approximately a factor of two. Further, the aspect ratio of the diffusion region does not change as the inflow density is lowered. Interestingly, the upstream magnetic field, however, is reduced as the density is lowered. The simulation results are used to empirically estimate the ion outflow speeds expected during magnetic reconnection in the magnetotail. Such an estimate is consistent with observations. In addition, we find a significant reduction in the quadrupole Hall magnetic fields in the diffusion region as well as an apparent enhancement of bipolar magnetic fields downstream inside the primary magnetic island.

II. SIMULATION METHODOLOGY

A PIC code[18,19] is used to carry out the simulations described here. We compute individual particle motions as coupled to Maxwells equations by solving the following normalized equations:

$$\frac{\partial \gamma \mathbf{v}_\alpha}{\partial t} = \frac{q_\alpha m_i}{m_\alpha}[\mathbf{E} + \mathbf{v}_\alpha \times \mathbf{B}], \tag{3}$$

$$\frac{\partial \mathbf{x}_\alpha}{\partial t} = \mathbf{v}_\alpha, \tag{4}$$

$$\frac{\partial \mathbf{B}}{\partial t} = -\nabla \times \mathbf{E}, \tag{5}$$

$$\frac{\partial \mathbf{E}}{\partial t} = \frac{c^2}{v_{A0}^2}(\nabla \times \mathbf{B} - \mathbf{J}), \tag{6}$$

$$\nabla \cdot \mathbf{E} = \frac{c^2}{v_{A0}^2}(n_i - n_e), \tag{7}$$

where c is the speed of light, γ is the Lorentz factor of special relativity, and $\alpha = i$, e represents ion and electron, respectively.

The electron mass m_e is normalized to ion mass m_i. Without losing generality, a value of $m_e = 0.04 m_i$ is chosen. Charges q are normalized to the elementary charge e. Therefore, $q_i = 1$ and $q_e = -1$ in the code. The initial equilibrium consists of two Harris sheets magnetic field $B_x(z) = B_\infty \tanh((z - L_z/4)/w_0) - B_\infty \tanh((z - 3L_z/4)/w_0) - 1$, where $B_\infty = 1$ is the asymptotic magnetic field value upstream and also the value magnetic fields are normalized to, L_z is the box size in Z, and w_0 is the width of the initial current sheets. The initial double Harris sheet density ensures pressure balance between the magnetic field and the thermal plasmas $n_x(z) = (1 - B_x(z)^2)/(2(T_i + T_e))$ everywhere in the simulation. Here, $T = T_i + T_e$ is the initial ion and electron temperatures, respectively. A background density n_b (normalized to the maximum value of the initial Harris sheets density n_0) is superimposed in the simulations. We can then, in principle, vary n_b to effectively vary the inflow density. Lengths (x, y, z) are normalized to an ion skin depth calculated from $d_{i0} = c/\omega_{pi0}$, where ω_{pi0} is the ion plasma frequency calculated from n_0. Time t is normalized to the inverse of ion cyclotron frequency Ω_{i0}^{-1} calculated from B_∞. The electric fields are normalized to $v_{A0}B_\infty/c$. The velocities are normalized to the referenced Alfvén speed $v_{A0} = B_\infty/(4\pi n_0 m_i)^{1/2}$. It can be calculated from the mass ratio, the density, and the magnetic field that in the initial Harris current sheet center, the electron plasma frequency over the electron Larmor frequency is $(\omega_{pe}/\Omega_{ce})_{Harris0} = 3$. In Eqs. (6) and (7), c/v_{A0} should be a uniquely determined value, a constant. However, for the same argument used for prescribing a representative m_e/m_i that is larger than the real value, we can similarly prescribe c/v_{A0} a value

that is smaller than its real value in order to save computational resource without losing generality, as long as $v_{A0} \ll c$.

Simulations in this paper are 2.5 dimensional and are performed in the X-Z plane. The positive Y direction is thus into the plane. The system is $102.4d_{i0} \times 102.4d_{i0}$. The grid scale is 0.05 d_{i0}. The initial current sheet width w_0 is chosen to be d_{i0}. For the background density equal 0.01 case, we put 5 particles into density the $n = 0.01$ cells, viz., 500 particles into $n = 1$ cells. Periodic boundary conditions are applied for both X and Z. The simulation is initialized with a double current of width $w_0 = d_{io}$ and small magnetic perturbations are included to introduce the tearing mode into the systems to initiate reconnections.[7] All simulations described in this paper are performed without a guide field. The ion and electron temperatures are set $T_i = 0.4167$ and $T_e = 0.0833$, respectively, where temperature T is normalized to a referenced temperature $T_0 = m_i v_{A0}^2$, and the ion mass $m_i = 1$. The speed of light is chosen to be $c = 15v_{A0}$. The code is relativistic to ensure that the electron velocity will not exceed the speed of light. We compare six simulations at background density $n_b = 0.01$, 0.015, 0.03, 0.1, 0.2, and 1.0. In addition, to ensure the validity of prescribing $c = 15v_{A0}$ for small inflow density simulations where the electron motion may be relativistic, we also perform simulations with $c = 30v_{A0}$ and $c = 45v_{A0}$ at smaller system sizes ($51.2d_{i0} \times 51.2d_{i0}$). We find that our choice of the speed of light does not affect the overall physical conclusions.

III. RESULTS

A. General properties

The double Harris-like current sheet system with periodic boundary conditions is chosen because it reproduces the large values of the tearing mode stability parameter Δ' (the jump of the derivative of A_{y1}, where A_{y1} is the out of plane displacement of the vector potential **A**) that characterize the long wavelength limit of reconnection in a single current slab[20] and does not exhibit artificial saturation due to conducting boundaries.[18] The two current sheets also produce two possible x-lines for study. Secondary magnetic islands periodically form during reconnection and have been found to modulate the reconnection rate,[21,22] although, our understanding of the role of the secondary islands in facilitating fast reconnection is still incomplete.[23,24] In this initial study of density dependence, we focus for simplicity on time periods where these secondary magnetic islands are not present. In comparing the results at various inflow densities, we sample all simulations at times when they reach the same level of reconnected flux ψ_B measured as the amount of magnetic flux between the X-line and the O-line. A value of $\psi_B = 10$ (in unit of $B_\infty d_{i0}$) is chosen for analysis because the reconnection is well developed in all cases, the primary magnetic island is large, but it is still early enough in time to ensure that the boundary conditions are not directly impacting the diffusion region.

Figure 1 shows the overviews of two extreme background density simulations: $n_b = 0.01$ and $n_b = 1.0$. Panel (a) compares the low density case to the high density case using the out of plane electron flow. For the low density case, the electrons diffusion region broadens significantly in Z due to the increase of the electron inertial length at a low density. Also, the in-plane flow is about 7–8 times faster. In the immediate outflow region, the flow structure is rather complex with a mix of in-plane and out-of-plane flows. The X-directional edge of the primary island is less defined with a fishbone (courtesy of William H. Matthaeus for coining the term) shaped instability being generated. The primary island is flattened out in X. This overview plot shows that the low density reconnection is a more violent physical process. As the local inertial length becomes larger, there is more room for kinetic instabilities and non-linear processes. In contrast, the high density case displays a relatively simpler physical picture that we are familiar with.

Figure 1(b) shows ion flow patterns in the X-Z plane via (v_{ix}, v_{iz}). The flow turn 90 deg from primarily in the v_z direction to primarily in the v_x direction through the ion diffusion region. For the low density case, this region broadens in both X and Z. Both the inflow and the outflow are faster. There is no apparent trace of the outflow wrapping around the downstream primary island, which is consistent with Panel (a) that the X-directional primary island in the low density case is less defined. In contrast, the high density case has a smaller ion diffusion region. The outflow deflects from the X direction to the Z direction to wrap around the downstream primary island. The downstream primary island is well defined with boundaries and significantly extends out of the initial current sheet in Z.

Figure 1(c) shows the out of plane magnetic field B_y. Note that both images are normalized to similar values on top of the panels. The quadrupole magnetic field in the low density case is significantly reduced due to the reduction of the hall currents whose magnitude scales as $|j_{hall}| \propto n_e v_e \propto n_e\sqrt{1/n_e} \propto \sqrt{n_e}$. Here we approximate electron flow v_e to scale with electron Aflvén speed as required by the whistler model associated with Hall physics.[25] In addition, for both low and high densities, relatively far downstream of the magnetic island, there is a bipolar B_y straddling the symmetry line along the X direction. This bipolar magnetic field is generated by a current j_x due to the streaming ions reflected off the pileup of B_z at the leading edge of the reconnection outflows. The leading edge of B_z has been termed "dipolarization fronts" in magnetotail studies.[26] The bipolar B_y is not seen in the high density case on the right column because the dipolarization front B_z in the high density case is reduced to a very small value that is not enough to reflect ions. In depth analysis of the dipolarization fronts for varying inflow densities is the subject of a manuscript in preparation.[27]

In Fig. 1, three panels of overview clearly show that inflow density plays a fundamental role in altering reconnection physics. Not only the scalings but also the physical processes involved are significantly modified. To study in detail, the quantitative aspect of the variations in reconnections, we first consider the reconnection rate E_R dependence on time, as shown in Fig. 2, where E_R is normalized to $v_{A0}B_\infty/c$. Clearly, results change drastically when we varied n_b. (1) The onset of reconnection is earlier for smaller background density simulations, e.g., $t_{start} \sim 56$, 80, 110, respectively, for

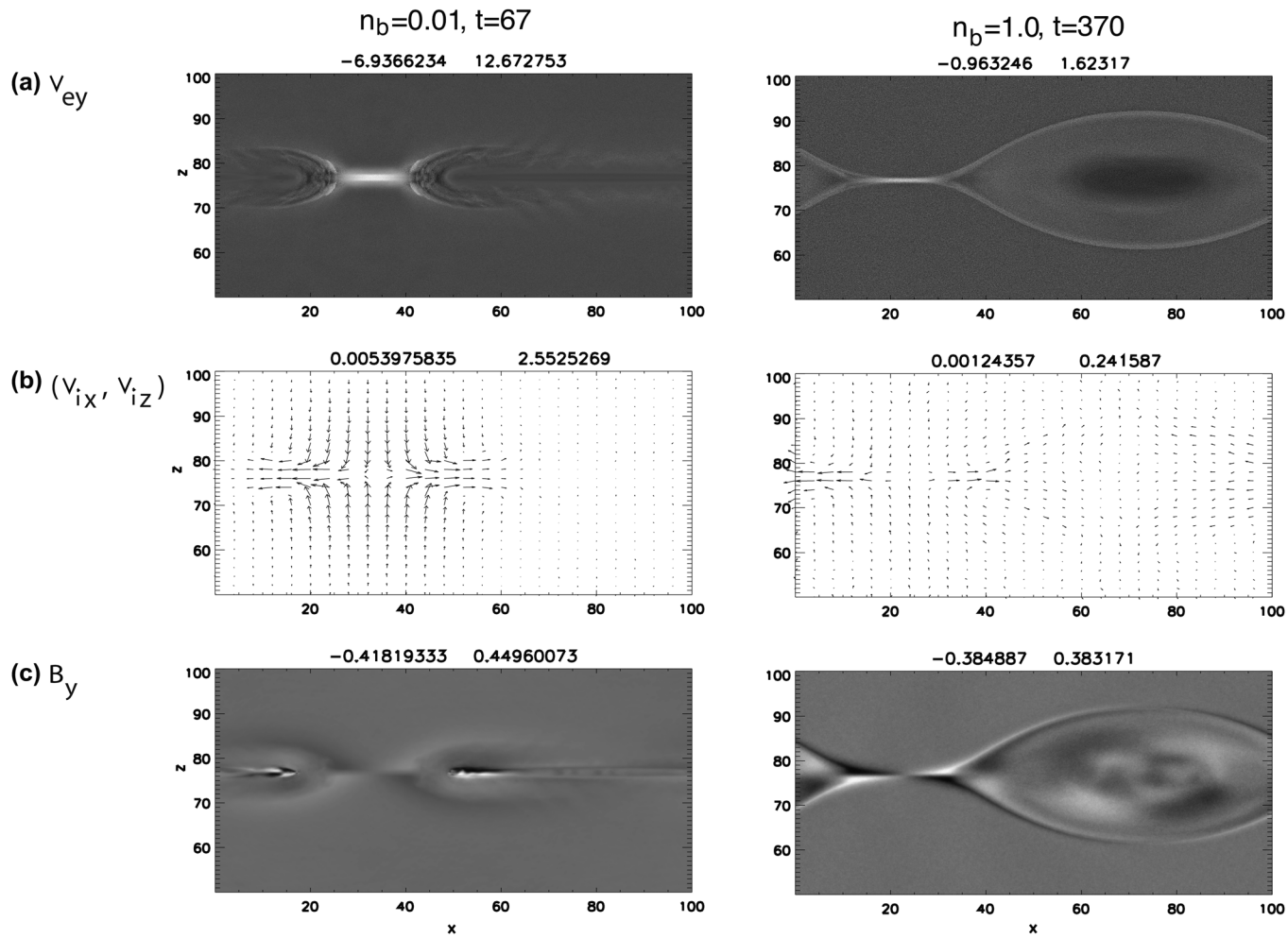

FIG. 1. Overview comparison of two extreme background density cases: $n_b = 0.01$ (left column) and $n_b = 1.0$ (right column) at times when the reconnected magnetic flux $\psi_B = 10$. (a) Electron out-of-plane flow v_{ey}, (b) ion in-plane flow vectors (v_{ix},v_{iz}), and (c) out-of-plane magnetic field B_y. The images are scaled to the maximum and minimum values marked on top of their respective panels, with white representing the maximum value and black representing the minimum value. Flow vectors in panel b scaled to maximum and minimum values given at the top of each plot.

the $n_b = 0.01$, 0.2, 1.0 cases. (2) The average reconnection rate is larger at a smaller inflow density. A conceptual explanation is that the upstream Alfvén speed $v_{A,up} \propto \sqrt{n_{up}}$

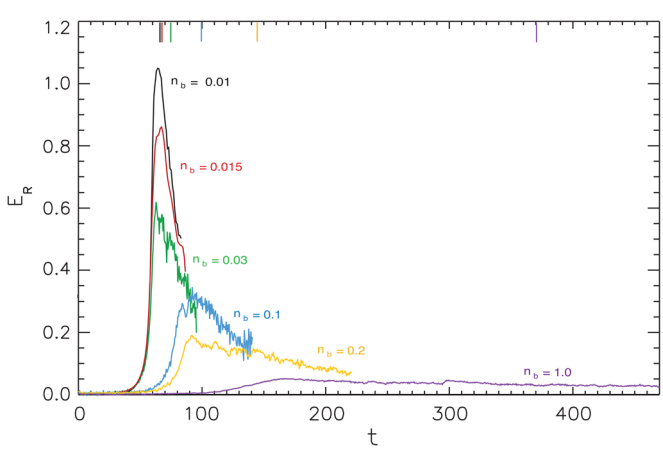

FIG. 2. (Color online) Reconnection rate E_R versus time. The background densities of the simulations are the $n_b = 0.01$, 0.015, 0.03, 0.1, 0.2, 1.0 simulations, respectively. The $n_b = 0.01$, 0.015 results are full precision data, the $n_b = 0.03$, 0.1, 0.2, 1.0 results are smoothed lower-precision. The times when the reconnected magnetic flux reach $\psi_B = 10$ are shown as vertical lines (also colored) at the top of the plot.

increases with a reduced inflow density. Hence, the outflow, which scales with $v_{A,up}$, becomes faster and the reconnection becomes faster. A quantitative explanation is more involved and is carried out later in the paper. (3) Reconnection lasts for a much longer time period at larger inflow densities, e.g., $\Delta t > 200$ for the $n_b = 1$ case, $\Delta t > 100$ for the $n_b = 0.2$ case, and $\Delta t = 20$ for the $n_b = 0.01$ case.

B. Diffusion region scaling analysis

Direct comparisons of the reconnection rates for different densities is not straightforward in this study because only the highest density cases exhibit periods of nearly steady reconnection. The other simulations show strong variations of the reconnection electric field E_R, with a sharp peak and then a declining reconnection rate. The peak in the reconnection rate occurs very early in time in the simulation, before the diffusion region is fully developed and is not appropriate for determining the structure of the diffusion region. We, therefore, examine the ion diffusion region for each simulation at a later time when the same amount of magnetic flux has reconnected, as in Sec. III A $\psi_B = 10$. There are well developed reconnection flows with a large primary magnetic

island. The reconnection outflows are far from reaching the simulation boundaries. The times when $\psi_B = 10$ are marked by vertical lines at the top of Fig. 2, which point systematically the decline of reconnection rate toward higher inflow densities.

Figure 2 provides one quantitative aspect of the diffusion region physics through the time-dependent and inflow-dependent reconnection electric field E_R. Another metric of the diffusion region is the scale of the ion diffusion region. Determination of the diffusion region structure for the different densities requires knowledge of the plasma properties just upstream of the diffusion region, B_{up} and n_{up}. These values can then be used in Eqs. (1) and (2). The upstream edge of the ion diffusion region can sometimes be determined by a direct comparison of E_y with $(\mathbf{v}_i \times \mathbf{B})_y$.[18] However, this method can be problematic in kinetic-PIC simulation due to particle noise. A proxy for this location is given by v_{iy}, which is caused by direct acceleration of unfrozen ions by the reconnection electric field. In the past, v_{iy} has been used successfully to determine the upstream edge of the ion diffusion region.[28] An example of how this method is applied is given in Fig. 3(a), which plots B_x and v_{iy} in a cut along Z through the X-line for the n = 1.0 case.

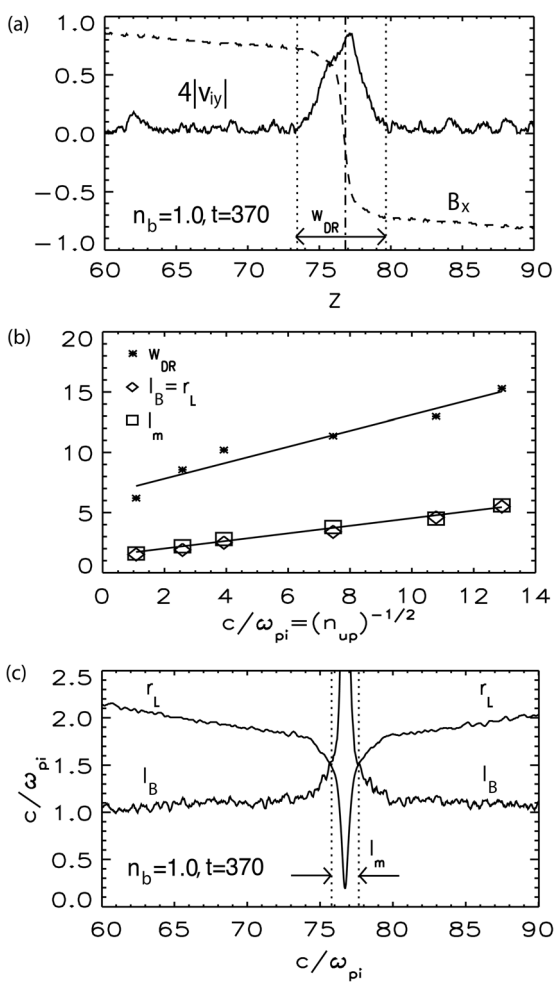

FIG. 3. (a) Determination of the diffusion region width. This is a cut along Z through the X-line from the $n_b = 1.0$ case: $4|V_y|$ (solid line) and B_x (dashed line). The X-line is marked by a dashed-dotted line and the edges of diffusion region are marked by dotted lines. (b) Lengths versus ion inertial length $c/\omega_{pi} = (n_{up})^{-1/2}$ (in simulation unit): diffusion region width w_{DR}, meandering width l_m, magnetic and Larmor scales at meandering width $l_{Bm} = r_{Lm}$. (c) Determination of meandering width: magnetic field length scale l_b and local Larmor radius r_L along Z through X-line.

In Fig. 3(a), we determine the upstream edges of the diffusion region to be about twice the distance from the X-line of where the out of plane ion flow velocities v_{iy} are half of their maximum values. We obtain the upstream magnetic field B_{up} (for anti-parallel reconnection, this is B_x) from the location of the upstream edge of the ion diffusion region. The upstream density n_{up} can also be obtained at the same locations.

The first diffusion region property to consider is its total width along the inflow direction w_{DR}. Since the ions decouple from the magnetic field when the Hall term in Ohm's law becomes significant, w_{DR} would be expected to scale with the ion inertial length c/ω_{pi}, giving $w_{DR} \sim (n_{up})^{-1/2}$. This scaling is consistent with simulations results as shown in Fig. 3(b). Another relevant scale length is the ion meandering length, determined by the kinetic bounce width of a typical ion.[29] Defining the magnetic field length scale $l_B = |B_x/(\partial B_x/\partial z)|$ and the local ion Larmor radius $r_L = v_{th}/\omega_{ci} = \sqrt{2T_{izz}/B_x}$, the meandering length of ions[30] in the diffusion region is determined by the two locations where $l_B = r_L$, as shown in Fig. 3(c) by l_m, which is twice the meandering length used in Ref. 30. At these locations we write $l_{Bm} = r_{Lm}$.

There are two striking features associated with the scaling of r_{Lm} and l_m: (1) r_{Lm} and l_m are almost equal for most densities and (2) l_m also scales with c/ω_{pi} as w_{DR} does. Since l_{Bm} is clearly associated with the distance from the diffusion region, its scaling with l_m follows, but the equality is quite surprising. The scaling of l_m with c/ω_{pi} follows from the fact that the Larmor radius of ions in the diffusion region is not set by the initial thermal velocity but by the ion inflow velocity, which scales with $v_{A,up}$ times a geometric factor. Inflowing ions form two counter-streaming populations at the x-line (Ref. 31, Fig. 7). For small enough temperature, the meandering orbit is set not by the thermal velocity of each population, but instead by the counter-streaming beam velocity, which gives $l_m \sim v_{A,up}/\omega_{ci} \sim c/\omega_{pi}$. The beam velocity, and not the thermal velocity, also controls the width of the electron diffusion region.[19] Therefore, in terms of understanding the scaling of the width of the ion diffusion region, the ion inertial length, and the ion meandering length are synonymous.

Repeating the procedure in Fig. 3 for the other simulations, we obtain the B_{up} and the n_{up} dependence on the background density n_b, as shown in Figs. 4(a) and 4(b). The figure shows $B_{up} \neq B_\infty$ and $n_{up} \neq n_b$. In fact, both B_{up} and n_{up} increase monotonically with increasing background density. We note that B_{up} ranges from 0.5 to 0.8 and it deviates more from its asymptotic value $B_\infty = 1$ when the background density is reduced. The reconnection rate E_R (same figure, Panel b, also measured at $\psi_B = 10$), on the other hand, increase monotonically with decreasing inflow density.

There is a critical question regards the aspect ratio δ/L of the ion diffusion region. Some previous studies have found that this aspect ratio is not changed as both d_{i0}/L and m_e/m_i are varied,[4,5] but its density dependence is unknown.

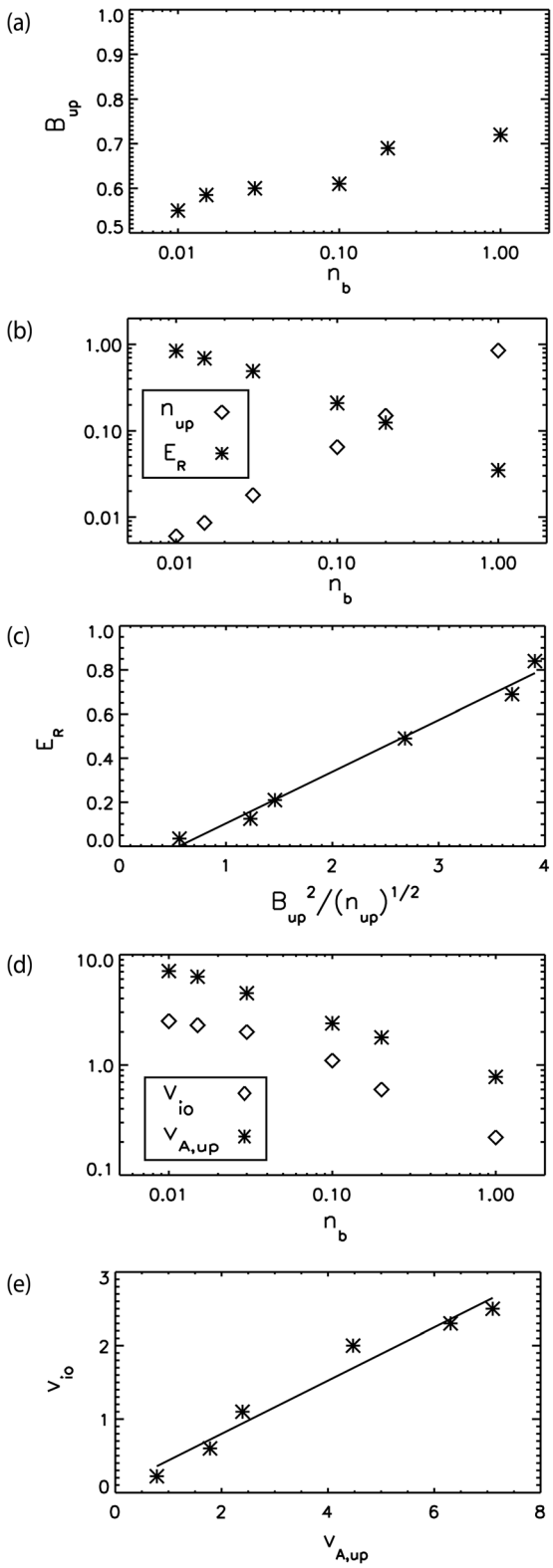

FIG. 4. (a) Log-linear scale: the upstream magnetic field B_{up} versus the background density n_b. (b) Log-log scale: the upstream density n_{up} and the reconnection rate E_R versus the background density n_b. (c) Slope of E_R versus $n_{up}{}^{1/2}/B_{up}{}^2$ gives diffusion region aspect ratio $\delta/L \sim 0.23 \pm 0.01$, a constant independent of the inflow density. (d) Log-log scale: the upstream Alfvén velocity $v_{A,up}$ and the downstream maximum ion outflow speed v_{io} versus the background density n_b. (e) v_{io} versus $v_{A,up}$.

Note that Eq. (2) can be rewritten as $E_R \sim (\delta/L) v_{A,up} B_{up}$, which when written in simulation normalized quantities yields $E_R \sim (\delta/L)(B_{up}^2/\sqrt{n_{up}})$. Thus, the slope of E_R versus $B_{up}^2/\sqrt{n_{up}}$ scales with the aspect ratio δ/L. In Fig. 4(c), the values from panels (a) and (b) are used to plot E_R versus $B_{up}^2/\sqrt{n_{up}}$. The values roughly lie on a straight line implying that the aspect ratio of the diffusion region is unchanged, independent of the inflow density. Here, this aspect ratio is calculated to be $\sim 0.23 \pm 0.01$ from the fitted line.

Figure 4(d) compares the scaling of the maximum ion outflow speed v_{io} as well as the upstream Alfvén speed $v_{A,up}$ at various background densities. Both velocities increase monotonically with decreasing background density. Plotting v_{io} versus $v_{A,up}$ in Fig. 4(e) reveals that they have a roughly linear relation: $v_{io} \approx 0.4 v_{A,up}$.

This diffusion region analysis provides a quantitative explanation for the increase in the reconnection rate as the background density decreases. With δ/L constant, then $E_R \sim B_{up}^2/\sqrt{n_{up}}$. Although B_{up} is reduced for smaller n_{up}, the $1/\sqrt{n_{up}}$ dominates giving a large increase in the outflow velocity and thus the reconnection rate.

IV. DISCUSSION

Particle simulations performed here focus on the quantitative scaling as well as the generic physics in the ion diffusion region of undriven magnetic reconnection, in the absence of a guide field. Varying the background density from 1 to 1/100th of the current sheet maximum density, we find that the diffusion region expands in both X and Z due to the increase of plasma inertial lengths. Such an expansion is in proportion to the inverse square root of the inflow density. The faster outflow (resulting from fast $v_{A,up}$) is the major reason for the increase of the reconnection rate by allowing faster transport. This is in spite of the fact that B_{up} decreases with decreasing n_{up}. The result is consistent with observational evidences that faster reconnections are associated with small inflow densities.[32–34]

The outflow velocity v_{out} continues to scale with the upstream Alfvén speed even in the low density cases. It appears that the pressure buildup due to the low density outflowing plasmas pushing the equilibrium current sheet density does not create a back pressure which modifies the diffusion region. The key here is that the ram pressure of the outflow: $P_{ram} \sim n v_{out}^2 \sim n v_{A,up}^2 \sim B_{up}^2$, due to the cancellation of density. The low density inflow is offset by a faster outflow velocity.

The aspect ratio of the diffusion region remains constant, independent of the reduced inflow densities and the enhanced reconnection electric field. This result implies that although the aspect ratio is a good measure of reconnection rate for many cases, it is not the only determining factor of reconnection rate. The reconnection electric field $E_R = \partial\psi_B/\partial t$ should also be considered in comparing reconnection rates, because E_R directly tells how much magnetic flux is being converted by magnetic reconnection per unit time.

There is a conundrum regarding measured magnetotail flows which are presumed to be due to magnetic reconnection. These flows typically range from 300 to 800 km/s.[35–37] Typical lobe magnetic fields are in the range B = 20–30 nT. While lobe densities are quite difficult to measure, estimates have placed a range of 0.007–0.092 cm^{-3} with the most likely value approximately 0.05 cm^{-3} in a recent publication.[13] The

average Alfvén speed in the lobe (using B = 25 nT, n = 0.05 cm^{-3} and Eq. (1)) is, therefore, 2400 km/s, which far exceeds typical flow measurements in the magnetotail.

Figure 4(e) provides at least a partial explanation for the disparity between the Alfvén speed and the measured outflows, as the reconnection velocity outflow in this study scales as roughly 0.4 of $v_{A,up}$. Reducing the average 2400 km/s speed by 0.4 gives a velocity of approximately 1000 km/s, which is still faster than a typical velocity, but much more reasonable.

In addition, the simulations with $n_b \approx 0.05$ show a reduction in B_{up} to about 0.6 of the asymptotic value. If it is assumed that the magnetic field upstream of the diffusion region is reduced to 0.6 of the lobe values, this yields a predicted outflow speed of approximately 600 km/s, which matches observations well. However, there is much uncertainty in this estimate as the reduction of B_{up} may have a strong system size and upstream boundary condition dependence. A more in depth study of the controlling factors in determining the scaling of outflow velocities is needed.

The reason as to why the reduced outflow velocity scaling factor ($v_{out} \sim 0.4 v_{A,up}$) is not clear. A low density pair plasma reconnection study found $v_{io} = 0.2 \sim 0.3 v_{A,up}$ which was attributed to a breakdown of the Sweet-Parker analysis.[15] This breakdown occurred because the fast time variation of the diffusion region violated the quasi-steady assumption necessary for a Sweet-Parker analysis. However, although there is fast time variation for the lower density cases in this study, both the low density and high density cases scale similarly. If quasi-steady was invalid for the low density cases, the scaling of velocity would be expected to change as the density was varied.

This scaling factor of 0.4 could be a natural consequence of basic conservation laws in the diffusion region as magnetic energy is converted into flows and heating. These conservation laws are utilized in the Sweet-Parker analysis of the diffusion region. However, different Sweet-Parker analysis have yielded factors ranging from $1/\sqrt{2}$ to $\sqrt{2}$ (e.g., Refs. 38–41 in the relation between v_{out} and $v_{A,up}$ owing to different assumptions about the spatial variation of quantities within the diffusion region as well as the effect of pressure.

Finally, kinetic effects within the diffusion region may be reducing the outflow velocity. For example, the mixing along magnetic field lines of accelerated and non-accelerated plasma in the diffusion region could effectively slow the outflow and cause the reduction in the scaling factor to 0.4.

Lastly, we find the reduction of the quadrupole magnetic field at small inflow densities. In fact, inflow density not only effects diffusion region physics but also alters downstream reconnection signatures, particularly the observables such as the dipolarization front (DF) in the Earth's magnetosphere. The DF, the bipolar magnetic field preceding the DF, and the DF related ion reflection/heating are out of the scope of this paper and are addressed in parallel in our other manuscript.[27]

ACKNOWLEDGMENTS

This work was supported by NSF Grant No. ATM-0645271 and NASA Grant Nos. NNX08AM37G and NNX08AO83G. Simulations were performed at the NCAR Computational Information Systems Laboratory, sponsored by NSF. P.W. thanks William Mattheaus, S. Peter Gary, Dan Winske, Naoki Bessho, Michael Hesse, Seiji Zenitani, Paul Cassak, Russel Kulsrud, Jonathan Eastwood, Kaijun Liu, Melvyn Goldstein, Jan Edgedal, and Anatoly Spitkovsky for discussions and encouragements.

[1]W. J. Hughes, "The magnetopause, magnetotail, and magnetic reconnection," in *Introduction to Space Physics*, edited by M. G. Kivelson and C. T. Russell (Cambridge University Press, New York, 1995), pp. 227–284.
[2]E. N. Parker, Astrophys. J. **264**, 642 (1983).
[3]J. A. Goetz, R. N. Dexter, and S. C. Prager, Phys. Rev. Lett. **66**, 608 (1991).
[4]M. A. Shay, J. F. Drake, and B. N. Rogers, Geophys. Res. Lett. **26**, 2163, doi:10.1029/1999GL900481 (1999).
[5]J. Birn, J. F. Drake, M. A. Shay, B. N. Rogers, R. E. Denton, M. Hesse, M. Kuznetsova, Z. W. Ma, A. Bhattacharjee, A. Otto, and P. L. Pritchett, J. Geophys. Res. **106**, 3715, doi:10.1029/1999JA900449 (2001).
[6]H. Karimabadi, W. Daughton, and J. Scudder, Geophys. Res. Lett. **34**, L13104 (2007).
[7]M. A. Shay, J. F. Drake, and M. Swisdak, Phys. Rev. Lett. **99**, 155002 (2007).
[8]M. Hesse, S. Zenitani, M. Kuznetsova, and A. Klimas, Phys. Plasmas **16**, 102016 (2009).
[9]D. Grasso, F. Pegoraro, F. Porcelli, and F. Galifano, Plasma Phys. Controlled Fusion **41**, 1497 (1999).
[10]X. Wang, A. Bhattacharjee, and Z. W. Ma, Phys. Rev. Lett. **87**, 265003 (2001).
[11]E. Fitzpatrick, Phys. Plasmas **11**, 937 (2004).
[12]A. Kuritsyn, H. Ji, S. P. Gerhardt, Y. Ren, and M. Yamada, Geophys. Res. Lett. **34**, L16106, doi:10.1029/2007GL030796 (2007).
[13]K. R. Svenes, B. Lybekk, A. Pedersen, and S. Haaland, Ann. Geophys. **26**, 2845 (2008).
[14]P. L. Prichett, J. Geophys. Res. **106**, 3794 (2001).
[15]N. Bessho and A. Bhattacharjee, J. Plasma Fusion Res. **5**, S2017 (2010).
[16]P. A. Sweet, "The neutral point theory of solar flares," in *Electromagnetic Phenomena in Cosmical Physics*, edited by B. Lehnert (Cambridge University Press, New York, 1958), pp. 123–134.
[17]P. Wu, M. A. Shay, T. D. Phan, M. Oieroset, and M. Oka, "Particle-in-cell simulation of magnetotail dipolarization fronts and associated ion reflection" (unpublished).
[18]M. A. Shay, J. F. Drake, and B. N. Rogers, J. Geophys. Res. **106**, 3759, doi:10.1029/1999JA001007 (2001).
[19]A. Zeiler, D. Biskamp, J. F. Drake, B. N. Rogers, M. A. Shay, and M. Sholer, J. Geophys. Res. **A9**, 1230, doi:10.1029/2001JA000287 (2002).
[20]D. Biskamp, *Magnetic Reconnection in Plasmas* (Cambridge University Press, Cambridge, England, 2000), pp. 99, 301.
[21]W. Daughton, J. Scudder, and H. Karimabadi, Phys. Plasma **13**, 072101 (2006).
[22]M. Oka, T. K. M. Nakamura, and K.-I. Nishikawa, Phys. Rev. Lett. **101**, 205004 (2008).
[23]W. Daughton, V. Roytershteyn, H. Karimabadi, L. Yin, B. J. Albright, S. P. Gary, and K. J. Bowers, AIP Conf. Proc. **1320**, 144 (2011).
[24]P. A. Cassak and M. Shay, Space Science Reviews (Springer, Netherlands, 2011), pp. 1–20.
[25]G. Pelletier, "Introduction to magneto-hydrodynamics,"in *Jets from Young Stars*, edited by C. D. Jonathan Ferreira and E. Whelan (Springer Berlin/Heidelberg, 2007), Vol. 723, p. 99.
[26]V. Angelopoulos, W. Baumjohann, C. F. Kennel, F. V. Coroniti, M. G. Kivelson, R. Pellat, R. J. Walker, H. Lohr, and G. Paschmann, J. Geophys. Res. **97**, 4027 (1991).
[27]P. Wu, M. A. Shay, T. D. Phan, M. Oieroset, and M. Oka, "Magnetotail dipolization front and associated ion reflection via particle-in-cell simulations," J. Geophys. Res. (unpublished).
[28]M. A. Shay, J. F. Drake, M. Swisdak, and B. N. Rogers, Phys. Plasmas **11**, 2199 (2004).
[29]W. Pei, R. Horiuchi, and T. Sato, Phys. Rev. Lett. **87**, 235003 (2001).
[30]A. Ishizawa and R. Horiuchi, Phys. Rev. Lett. **95**, 045003 (2005).

[31]M. A. Shay, J. F. Drake, R. E. Denton, and D. Biskamp, J. Geophys. Res. **103**(A5), 9165, doi:10.1029/97JA03528 (1998).
[32]C. T. Russell, Geophys. Res. Lett. **27**(20), 3257, doi:10.1029/2000GL011910 (2000).
[33]V. M. Mishin, T. Saifudinova, A. Bazarzhapov, C. T. Russell, W. Baumjohann, R. Nakamura, and M. Kubyshkina, J. Geophys. Res. **106**, 13, doi:10.1029/2000JA900152 (2001).
[34]X. Cao, Z. Y. Pu, H. Zhang, V. M. Mishin, Z. W. Ma, M. W. Dunlop, S. Y. Fu, L. Xie, C. J. Xiao, X. G. Wang, Q. G. Zong, Z. X. Liu, M. V. Kubyshkina, T. I. Pulkkinen, H. U. Frey, A. Korth, M. Fraenz, E. Lucek, C. M. Carr, H. Reme, I. Dandouras, A. N. Fazakerley, G. D. Reeves, R. Friedel, K. H. Glassmeier,, and C. P. Escoubet, J. Geophys. Res. **113**, A07S25, doi:10.1029/2007JA012761 (2008).
[35]A. Raj, J. Geophys. Res. **107**, 1419, doi:10.1029/2001JA007547 (2002).
[36]V. Angelopoulos, J. P. McFadden, D. L. C. W. Carlson, S. B. Mende, H. Frey, T. Phan, D. G. Sibeck, K.-H. Glassmeier, U. Auster, E. Donovan, I. R. Mann, I. J. Rae, C. T. Russell, A. Runov, X.-Z. Zhou, and L. Kepko, Science **321**, 931 (2008).
[37]J. P. Eastwood, T.-D. Phan, M. Oieroset, and M. A. Shay, J. Geophys. Res. **115**, A08215, doi:10.1029/2009JA014962 (2010).
[38]M. Hesse, J. Birn, and S. Zenitani, Phys. Plasmas **18**, 042104 (2011).
[39]M. Swisdark and J. F. Drake, Geophys. Rev. Lett. **34**, L11106, doi:10.1029/2007GL029815 (2007).
[40]P. A. Cassak and M. A. Shay, Phys. Plasma **14**, 102114 (2007).
[41]E. Priest and T. Forbes, *Magnetic Reconnection: MHD Theory and Applications* (Cambridge University Press, New York, 2000).